Integrated thermal stabilization of a microring modulator

Kishore Padmaraju,[1,*] Dylan F. Logan,[2,3] Xiaoliang Zhu,[1] Jason J. Ackert,[2] Andrew P. Knights,[2] and Keren Bergman[1]

[1]*Department of Electrical Engineering, Columbia University, 500 West 120th Street, New York, New York, USA*
[2]*Department of Engineering Physics, McMaster University, 1280 Main Street West, Hamilton, ON, Canada*
[3]*Department of Electrical and Computer Engineering, University of Toronto, 10 King's College Rd., Toronto, ON, Canada*
[*]*kpadmara@ee.columbia.edu*

Abstract: A defect-enhanced silicon photodiode and heater are integrated with and used to thermally stabilize a microring modulator. These optoelectronic components are interfaced with external control circuitry to create a closed-looped feedback system for thermally stabilizing the microring modulator. The thermal stabilization system enables the microring modulator to provide error-free 5-Gb/s modulation while being subjected to thermal fluctuations that would normally render it inoperable.

©2013 Optical Society of America

OCIS codes: (230.4110) Modulators; (230.4555) Coupled resonators; (200.4650) Optical interconnects.

References and links

1. A. V. Krishnamoorthy, R. Ho, X. Zheng, H. Schwetman, J. Lexau, P. Koka, G. Li, I. Shubin, and J. E. Cunningham, "Computer systems based on silicon photonic interconnects," Proc. IEEE **97**(7), 1337–1361 (2009).
2. N. Ophir, D. Mountain, C. Mineo, and K. Bergman, "Silicon photonic microring links for high-bandwidth-density, low-power chip I/O," IEEE Micro **33**(1), 54–67 (2013).
3. W. A. Zortman, A. L. Lentine, D. C. Trotter, and M. R. Watts, "Bit error rate monitoring for active wavelength control of silicon microphotonic resonant modulators," IEEE Micro **33**(1), 42–52 (2013).
4. K. Padmaraju, J. Chan, L. Chen, M. Lipson, and K. Bergman, "Thermal stabilization of a microring modulator using feedback control," Opt. Express **20**(27), 27999–28008 (2012).
5. M. W. Geis, S. J. Spector, M. E. Grein, J. U. Yoon, D. M. Lennon, and T. M. Lyszczarz, "Silicon waveguide infrared photodiodes with >35 GHz bandwidth and phototransistors with 50 AW^{-1} response," Opt. Express **17**(7), 5193–5204 (2009).
6. R. R. Grote, K. Padmaraju, B. Souhan, J. B. Driscoll, K. Bergman, and R. M. Osgood, Jr., "10 Gb/s error-free operation of all-silicon ion-implanted-waveguide photodiodes at 1.55 μm," IEEE Photon. Technol. Lett. **25**(1), 67–70 (2013).
7. D. F. Logan, P. Velha, M. Sorel, R. M. De La Rue, P. E. Jessop, and A. P. Knights, "Monitoring and tuning micro-ring properties using defect-enhanced silicon photodiodes at 1550 nm," IEEE Photon. Technol. Lett. **24**(4), 261–263 (2012).
8. K. Padmaraju, D. F. Logan, X. Zhu, J. J. Ackert, A. P. Knights, and K. Bergman, "Integrated thermal stabilization of a microring modulator," *Proc. Optical Fiber Communication Conference* (Optical Society of America, 2013), paper OM2H.7.
9. J. Teng, P. Dumon, W. Bogaerts, H. Zhang, X. Jian, X. Han, M. Zhao, G. Morthier, and R. Baets, "Athermal silicon-on-insulator ring resonators by overlaying a polymer cladding on narrowed waveguides," Opt. Express **17**(17), 14627–14633 (2009).
10. W. A. Zortman, A. L. Lentine, D. C. Trotter, and M. R. Watts, "Integrated CMOS compatible low power 10Gbps silicon photonic heater-modulator," *Proc. Optical Fiber Communication Conference* (Optical Society of America, 2012), paper OW4I.5.
11. V. Michal, C. Premont, G. Pillonet, and N. Abouchi, "Single active element PID controllers," *Radioelektronika, 2010 20th International Conference*.
12. Y.-H. Chen, C. Sun, and V. Stojanovic, "Scalable electrical-optical thermal simulator for multicores with optical interconnects," *Proc. IEEE Optical Interconnects Conference* (IEEE, 2013), paper MA3.
13. C. J. B. Fayomi, M. Sawan, and G. W. Roberts, "Reliable circuit techniques for low-voltage analog design in deep submicron standard CMOS: a tutorial," Analog Integr. Circuits Signal Process. **39**(1), 21–38 (2004).

14. D. Brunina, X. Zhu, K. Padmaraju, L. Chen, M. Lipson, and K. Bergman, "10-Gb/s WDM optically-connected memory system using silicon microring modulators," *Proc. European Conference on Optical Communications* (Optical Society of America, 2012), paper Mo.2.A.5.
15. D. Livshits, D. Yin, A. Gubenko, I. Krestnikov, S. Mikhrin, A. Kovsh, and G. Wojcik, "Cost-effective WDM optical interconnects enabled by quantum dot comb lasers," *Proc. Optoelectronic Interconnects and Component Integration IX* (SPIE, 2010).
16. A. V. Krishnamoorthy, X. Zheng, G. Li, J. Yao, T. Pinguet, A. Mekis, H. Thacker, I. Shubin, Y. Luo, K. Raj, and J. E. Cunningham, "Exploiting CMOS manufacturing to reduce tuning requirements for resonant optical devices," IEEE Photon. J. **3**(3), 567–579 (2011).
17. M. Georgas, J. Leu, B. Moss, C. Sun, and V. Stojanovic, "Addressing link-level design tradeoffs for integrated photonic interconnects," in *Custom Integrated Circuits Conference* (IEEE, 2011), 978–1-4577–0233–5/11.
18. P. Dong, W. Qian, H. Liang, R. Shafiiha, D. Feng, G. Li, J. E. Cunningham, A. V. Krishnamoorthy, and M. Asghari, "Thermally tunable silicon racetrack resonators with ultralow tuning power," Opt. Express **18**(19), 20298–20304 (2010).

1. Introduction

Growing bandwidth demand has made necessary the use of optical communications at unprecedented small scales and distances, in scenarios such as rack-to-rack links in data centers, board-to-board interconnects, and ultimately for use within multi-core processors [1]. However, at these reduced scales, optical links are only feasible if they can be realized in a small footprint and energy-efficient manner. For this reason, the silicon photonics platform, with its ability to manifest CMOS-compatible photonic devices, is promising for use in next-generation optical links. In particular, microring-based silicon photonic devices have been shown to push the boundaries on the aforementioned metrics of size and energy efficiency [2].

However, as the high-performance functionality of both passive and active microring-based devices have continued to be demonstrated, concerns have grown over the suitability of these devices for use in thermally volatile environments. The high thermo-optic coefficient of silicon, combined with the resonant nature of the microring-based devices, makes the operation of said devices susceptible to thermal fluctuations of only a few kelvin (K) [3]. Additionally, due to fabrication variation, the initial wavelength position of the microring resonance needs to be adjusted to match the operating wavelength of the optical path.

The most promising efforts at resolving this problem have involved the use of control systems [3,4]. In particular, it was shown that using a control system, a microring modulator could maintain error-free performance under thermal fluctuations that would normally render it inoperable [4]. A control system thermally stabilizes the microring modulator by monitoring the temperature, either directly or indirectly, and then adjusting the local temperature of the modulator using an appropriate mechanism. In the cited demonstration [4], changes in the temperature of the microring modulator were inferred by monitoring the mean power of the microring-modulated signal using an off-chip photodetector. To complete the control system, the bias current was varied to provide the necessary temperature adjustment in the localized region of the microring modulator.

In this demonstration, we further the results of [4] by showing that the optoelectronic components that comprise the control system can be integrated onto a single device using CMOS-compatible processes and materials. The enabling technology of this integration is the use of a defect-enhanced silicon photodiode [5]. Such devices have been demonstrated as effective high-speed optical receivers [6], but an additional utility lies in their use as in situ power monitors for silicon photonic devices [7]. Positioned on the drop-port of the microring modulator, the silicon photodiode is utilized as the photodetector neccessary to monitor the mean power of the modulated signal. This configuration avoids the use of a power tap and is compatible with the wavelength-division-multiplexed (WDM) arrangement of microring modulators, in which several microrings are cascaded along the same waveguide bus.
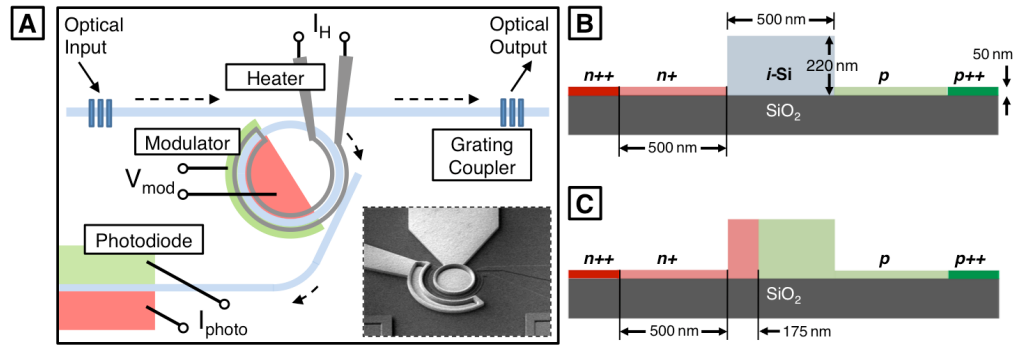
Fig. 1. (a) Schematic of the integrated device (not to scale), and SEM image of fully processed device (inset). Waveguide geometry and doping profile for the (b) silicon photodiode and (c) depletion-mode microring modulator.

The layout of the integrated device is shown in Fig. 1(a), and consists of a depletion-mode microring modulator, with a thin film heater directly above it, and a defect-enhanced silicon photodiode on the drop-port. Holographic gratings of 70-nm etch depth are employed to facilitate coupling of C-band wavelengths into and out of the chip. The ring is 15 µm in radius, and has a 210 nm point-coupling gap to the input and drop-port waveguide. The cross-section of the photodiode and modulator are shown in Fig. 1(b) and 1(c), respectively. The waveguides are 500 nm wide and 220 nm in height, and etched to a depth of 170 nm. The modulator is formed of an n^+p junction that takes up one-half of the ring circumference. The p-side of the junction is composed of a uniform boron concentration of 5×10^{17} cm^{-3} and the n^+-side of the junction is composed of a uniform phosphorus concentration of 1×10^{18} cm^{-3}. The junction is offset by 75 nm from the center of the waveguide. The thin film heater is patterned on a 180-nm thick titanium-based layer separated from the active layer by 1.2 µm of oxide. The photodiode is 500 µm long, and consists of a p-i-n^+ junction formed laterally on the waveguide. The p and n^+ doping levels of the modulator are in this case aligned to the edge of the waveguide, leaving the core undoped. Sensitivity to sub-bandgap wavelengths was provided by deep level lattice defects introduced by a masked phosphorus implantation of 300 keV and 1×10^{13} cm^{-2} dose followed by a 10 min anneal at 475 °C in a N$_2$ ambient. The damage implantation and anneal was performed directly prior to the metal heater deposition in the process flow.
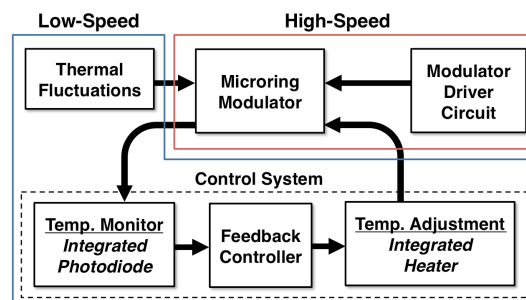
Fig. 2. Schematic of the control system, highlighting the separation of the high-speed data transmission from the low-speed stabilization of thermal fluctuations.

Figure 2 outlines the control system, indicating how the integrated components work in conjunction to thermally stabilize the microring modulator. As is typical, the microring modulator is driven by a high-performance high-speed driver circuit to generate Gb/s optical data. On a much slower scale, thermal fluctuations in the environment will cause the

temperature of the microring modulator to change, negatively impacting the performance of the microring modulator.

To keep the microring modulator thermally stabilized, the integrated photodiode on the drop port is first used to ascertain changes in the temperature of the microring modulator. As established in [4], changes in the mean power of the modulated-signal can be used to detect shifts in the temperature of the microring modulator. Figure 3(a) shows measurements of the voltage generated by the drop-port photodiode. When the microring is in its electrically passive state, the drop-port photodiode generates the expected photoresponse, mirroring the lorentzian lineshape of the microring's optical resonance. When the microring is modulated, the photodiode generates a photocurrent equivalent to the average power between the '1' and '0' modulation states [4]. The resulting broadened response can be seen in Fig. 3(a). Additionally, the generated 5-Gb/s eye diagrams for several wavelength points are indicated in Fig. 3(b)-3(e). Highlighted in red on the photoresponse curve of Fig. 3(a) is a region that produces optimally modulated data (Fig. 3(d)). This region of monotonic slope is used to ascertain changes in temperature. Once the reference is set in the region, increases or decreases in temperature will cause the curve to shift higher or lower in wavelength, respectively, and subsequently result in an increase or decrease of the photosignal.
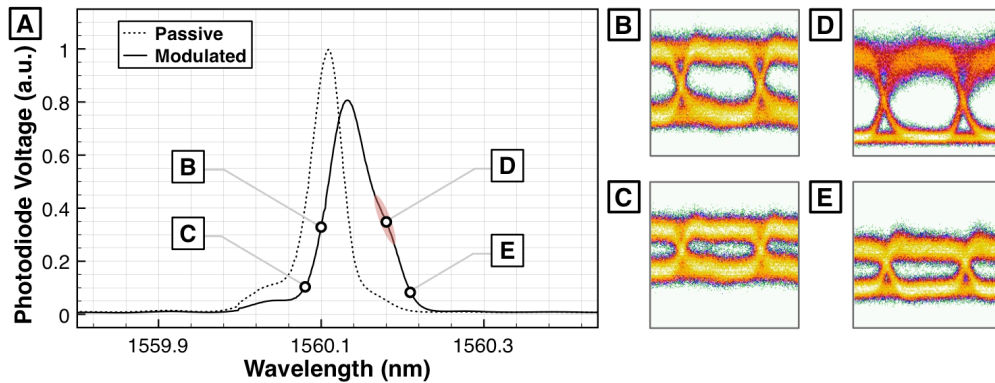
Fig. 3. (a) Measured photoresponse of the drop-port photodiode for when the microring is in its passive state, as well as for when it is modulated. (b-e) Generated 5-Gb/s eye diagrams as indicated at several points on the measured photoresponse of the modulated microring.

Once the temperature change has been inferred by the integrated photodiode, the integrated heater can then maintain the temperature of the microring modulator by increasing or decreasing its thermal output in response to a decrease or increase of the ambient temperature, respectively. A feedback controller interfacing the two components maintains closed-looped operation of the system (illustrated in Fig. 2). Using this control system, the local temperature of the microring modulator is held constant, and its high-speed performance continues uninterrupted.

As highlighted in Fig. 2, an important aspect of this integrated system is the independent operation of the low-speed thermal stabilization from the high-speed optical modulation. The control system operates on the same temporal scale as the generation of thermal fluctuations. An important consequence of this is that the control system can be composed of low-speed, and subsequently, energy-efficient electronics that are separate from the high-performance electronics driving the microring modulator.

2. Experimental results

In our experimental setup [Fig. 4(a)], a pulsed-pattern-generator was used to generate a 5 Gb/s non-return-to-zero (NRZ) 2^7-1 pseudo-random-bit-sequence (PRBS) electrical signal (we have previously demonstrated the system with 2^{31}-1 PRBS as well [8]). This electrical

signal was amplified to 5 Vpp and biased at −5 V to drive the microring modulator using high-speed electrical probes (a Picoprobe by GGB Industries, Inc.). A separate set of low-speed electrical probes was used to contact the heater and silicon photodiode. A CW tunable laser was set to TE polarization before being launched into the grating coupler with a power of 3 dBm. The microring-modulated 5 Gb/s optical signal was recovered from the exit grating coupler for bit-error-rate (BER) measurements and eye diagrams.

To simulate thermal fluctuations, the localized region of the microring modulator was excited from above by a 647-nm visible laser [4]. The power of the visible laser was internally modulated from 10 Hz – 100 Hz to generate ensuing thermal fluctuations of the same frequency, and of magnitude 3 K, in the region of the microring modulator.
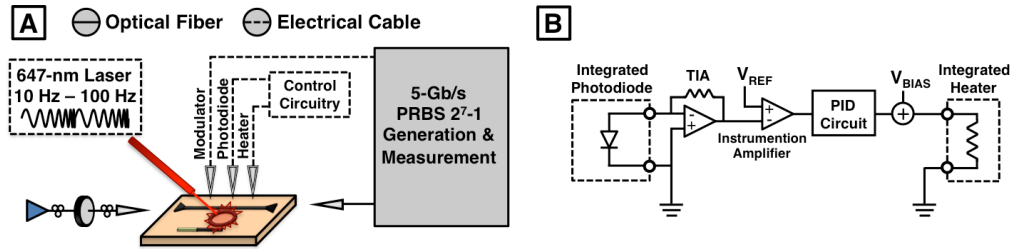
Fig. 4. (a) Experimental setup. The 647-nm visible laser is used to simulate thermal fluctuations. (b) Circuitry comprising the control system. Indicated in the dashed boxes are the on-chip integrated components.

As Fig. 4(a) shows, the operation of the control system occurs independent of the high-speed operation of the microring modulator. Figure 4(b) outlines the control circuitry, including the interface between the circuitry and the on-chip integrated photodiode and heater. As previously mentioned, the silicon photodiode is used to ascertain changes in the mean power of the modulated optical signal. The photodiode current is fed into an op-amp transimpedance-amplifier (TIA) circuit that produces a voltage corresponding to the amount of optical power received by the silicon photodiode. The transimpedance voltage generated from this arrangement is then compared to a reference voltage using an instrumentation amplifier. The resultant error signal is fed into an analog proportional-integral-derivative (PID) control circuit. The PID circuit generates a feedback signal that is used to adjust the voltage on the integrated heater. A bias voltage (V_{BIAS} in Fig. 4(b)) is also used to set the microring modulator's operating point to an initial wavelength.
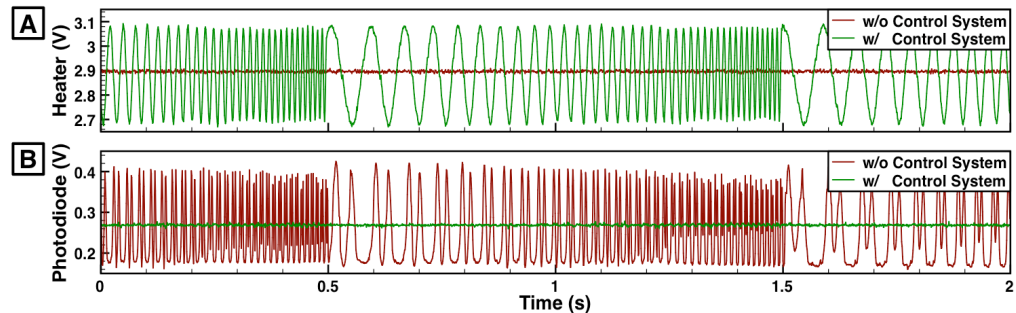
Fig. 5. Oscilloscope measurements (with and without the control system) of the (a) voltage applied to the heater, and the (b) voltage generated from the photodiode (following the TIA) measuring the mean modulation power.

Through the described mechanism, the integrated heater dynamically reduces current (cools down) in the presence of high ambient temperatures and increases current (heats up) in the presence of low ambient temperatures, thereby maintaining the temperature of the

microring modulator at a set operating temperature throughout the duration of the thermal fluctuations inflicted by the visible laser.

The dynamic adjustment of the heater voltage is seen in the oscilloscope trace of Fig. 5(a). Without the control circuit, the heater voltage is set at a constant 2.9 V (an arbitrary voltage), whereas, with the control circuit, the voltage is swung dynamically between 2.7 V and 3.1 V to correct for the thermal fluctuations afflicting the microring modulator. The effect of this action can be seen in the transimpedance voltage from the photodiode [Fig. 5(b)], which was used to measure the mean power of the optical signal in our control system. Without the control system the mean power fluctuates in correspondence with the thermal fluctuations. The control system locks the mean power to the set reference, ensuring that the modulation is maintained throughout the duration of the thermal fluctuations.

The resonance tuning efficiency of the integrated heater was measured to be 0.12 nm/mW. Utilizing a calculation of the group index of the waveguide, the thermal sensitivity of the resonance is 0.072 nm/K (8.9 GHz/K) [9]. From measuring the minimum and maximum voltage needed to thermally stabilize the microring modulator [Fig. 5(a)], the magnitude of the temperature fluctuation is inferred to be 3 K. This was the maximum temperature fluctuation that we could generate using the visible laser. While this modest temperature fluctuation is enough to demonstrate the functionality of the stabilization system, it does not represent the full temperature range that the system would be able to correct for. The real limit on the temperature range of the system is the tuning range is the integrated heater, which we were able to routinely tune upwards of 50 K.
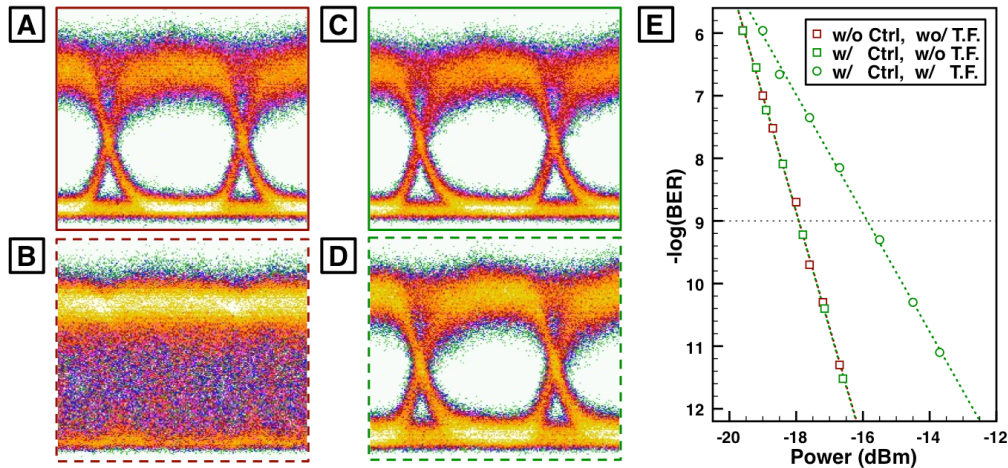
Fig. 6. Eye diagrams of 5-Gb/s microring-modulated optical signal *without* the control system (Ctrl) in (a) a stable thermal environment, and (b) under thermal fluctuations (T.F.). Similarly, the microring modulation *with* the control system in (c) a stable thermal environment, and (d) under thermal fluctuations. (e) BER measurements corresponding to eye diagrams in (a), (c), and (d).

The eye diagrams and BER measurements in Fig. 6 validate the performance of the control system. Without the thermal fluctuations, there is a negligible difference between operating the microring modulator without control [Fig. 6(a)], and with control [Fig. 6(c)], further confirmed by the BER measurements in Fig. 6(e), which shows that there is no incurred power penalty as a consequence of operating with the control system. As seen in Fig. 6(b), subjection of the microring modulator to thermal fluctuations without corrective feedback tuning will result in complete failure of the modulation. However, as can be seen in Fig. 6(d), the control system can completely correct for the thermal disturbances, maintaining error-free (defined as a 10^{-12} error-rate) modulation with a power penalty of 2 dB (in comparison to the back-to-back case of Fig. 6(a)).

The 2-dB power penalty is attributable to mode-hopping in the visible laser inflicting the thermal fluctuations. The large modulation of current of the visible laser causes it to mode-hop, resulting in small but fast discontinuities in the modulation of its optical power. This results in small but very fast thermal fluctuations appearing in the larger overall thermal fluctuation. We designed our circuitry to counteract thermal fluctuations < 1 kHz, implementing low-pass filters to reduce the noise in our unshielded circuitry. As a consequence, it could not contend with these small but fast mode-hopped induced thermal fluctuations, creating the large 2-dB power penalty. If the control system were to be properly implemented in integrated circuitry, we envision that the 2-dB power penalty would be drastically reduced.

3. Energy efficiency analysis

For the successful implementation of our thermal stabilization system in commercial applications the system must adhere to the stringent power consumption requirements foreshadowed for future small-scale optical interconnects. These predictions project that in the most demanding environments, the justification for optical networks-on-chip will require the aggregate power consumption for the optical link to be below ~1 pJ/bit [1]. Less localized interconnects, such as the ones that will populate board-to-board or rack-to-rack interconnections will likely be less strict. To validate the feasibility of our demonstrated system, we project its power consumption if implemented with current leading technology.

As shown in Fig. 2, the thermal stabilization system is composed of sub-components, the first sub-component consisting of circuitry to extract the photodiode current and condition the feedback response, the second sub-component consisting of the resistive heater used to adjust the local temperature of the microring modulator.

For the integrated heater used in our device, we measured a DC resistance of 1340 Ω, and a tuning efficiency of 0.12 nm/mW (67 µW/GHz). This integrated heater was not optimized for tuning efficiency, and hence, has a relatively low tuning efficiency when compared to more recent literature. For this reason, in our analysis we utilize the results of [10], in which an integrated heater was demonstrated to tune across 5 nm (64 K), using sub 1-V voltage, a tuning efficiency of 1.14 nm/mW (7 µW/GHz), and without compromising the performance of the 10-Gb/s microring modulator.

For analyzing the power consumption of the circuitry, we reference Fig. 4(b), where it is illustrated how the circuitry is composed of a TIA, instrumentation amplifier, PID control circuit, and summer. Aside from the instrumentation amplifier, all of these components were implemented using standard op-amps. However, the instrumentation amplifier is internally composed of 3 op-amps, and can be deconstructed into such. While we used individual op-amps for the proportional, derivative, and integral portions of the PID control, the entire PID control can be, and is routinely implemented, as a single op-amp circuit [11]. Hence, the circuit can be reduced to a total of 6 op-amps.

Simulations on deeply integrated silicon photonic components have shown thermal time constants on the order of ~1 ms [12]. We have shown previously that a feedback controller implemented in analog electronics, comprised of op-amps of 3-MHz bandwidth, could stabilize against thermal fluctuations > 1 kHz [4]. Hence, we conclude that op-amps used in an integrated microelectronic implementation of the system would need to have a bandwidth on the order of 1 MHz, while being able to supply the 1 V required to maximally tune the aforementioned integrated heater [10]. Fortunately, op-amps with these characteristics have been routinely implemented in CMOS technology, with power consumptions as low as 40 µW [13]. This yields an aggregate power consumption of 24 fJ/bit of the circuit at a microring modulation speed of 10 Gb/s.
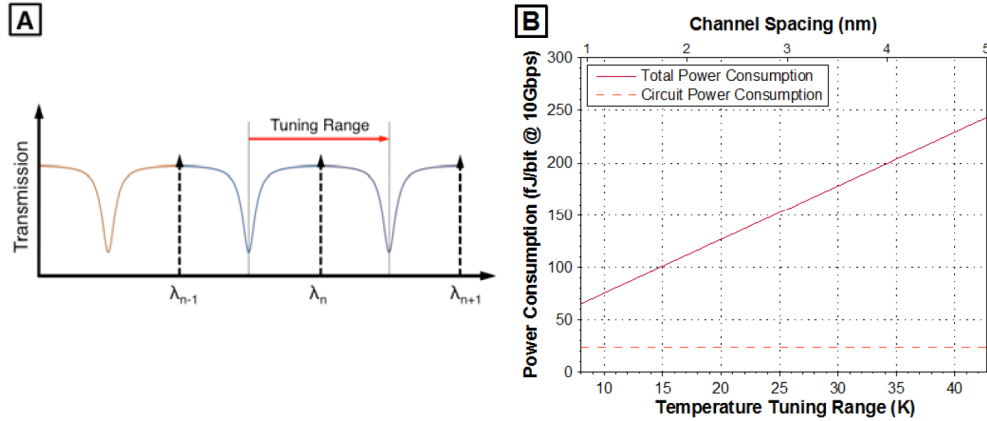
Fig. 7. (a) Diagram of an array of microring resonators and a comb laser source with equivalent spacing. Ambient temperature changes will create relative offsets between the two grids, but this can be corrected by tuning the microring to the laser, with the maximum tuning range equivalent to the channel spacing (the microring-wavelength arrangement will be reshuffled if the microring needs to tune past this point). (b) Estimated average power consumption for thermally stabilizing a single microring modulator. For larger channel spacings (top axis), the microring modulator may have to be tuned across a larger temperature range (bottom axis).

To fully leverage the advantages of microrings, future optical interconnects will likely utilize them in a WDM configuration, cascaded along the same waveguide bus [14]. The source for this type of system will likely be a comb laser containing evenly spaced channels [15]. Additionally, advances in process technology have demonstrated evenly channel-spaced microrings within localized regions [16]. Hence, it is possible to engineer a system in which there is a rigidly channel-spaced laser source, a rigidly & equivalently channel-spaced array of microring modulators, and a slight offset between the two WDM grids from ambient temperature changes.

Lastly, we note schemes to minimize the maximum tuning range of any single microring modulator. Specifically, if the temperature change is large enough to shift the microrings more than one channel spacing of their original position, the microring-wavelength assignments can be reshuffled to minimize tuning [17]. Hence, as depicted in Fig. 7(a), the maximum tuning range required for a single microring modulator will be equivalent to the channel spacing. In the outlined system, the power consumption for thermally stabilizing a single modulator will be, on average, $P_{Total} = P_{Circuit} + 0.5*Max\{P_{Heater}\}$, where $P_{Circuit}$ is relatively static, and $Max\{P_{Heater}\}$ is the maximum required power expended by the heater. Utilizing the previous metrics and analysis, Fig. 7(b) plots the average power consumption of the thermal stabilization system as a function of channel spacing (top axis), or equivalently, the maximum temperature tuning range required for that channel spacing (bottom axis).

The plot in Fig. 7(b) shows that the integrated heater comprises the large bulk of the power consumption, especially when it is required to cover a large tuning range. While [10] is a leading demonstration of heater efficiency for microring modulators, there may be ways to extend the efficiency of integrated heaters further, such as using undercut structures, for which tuning efficiencies of 2.7 nm/mW (3 µW/GHz) have been demonstrated for passive microring resonators [18]. Improvements in the tuning efficiency of integrated heaters would drastically reduce the power consumption of the thermal stabilization system.

4. Discussion and conclusion

We have demonstrated a thermal stabilization system that maintains the error-free performance of a microring modulator when it is subjected to thermal fluctuations of 3 K, a

magnitude that would normally render it inoperable. While, in this instance, the stabilization system was tested for thermal fluctuations, it operates equally well, and without any modifications, for fluctuations in the wavelength of the laser source, assuming such fluctuations are on a similar time scale. This bit-rate transparent stabilization system operates independently, and without disturbing, the high-performance optical modulation. All the optoelectronic components necessary to implement the stabilization system have been integrated onto a single device using CMOS-compatible processes.

A clear advantage of the system is that no optical power taps are needed [4]; the unused power in the drop port is recycled to provide the mean power detection. Additionally, this type of implementation is compatible with the WDM configuration of microring modulators.

In our demonstration, we utilized external low-speed analog electronics to implement the control circuitry in the stabilization system. The use of low-speed analog electronics validates the simplicity of the solution, and as our energy efficiency analysis showed, when implemented in standard CMOS VLSI technology, the power consumption of the circuitry will be able to adhere to the most stringent power requirements.

The range of thermal fluctuations that our system was demonstrated for was limited by our experimental implementation. In a packaged solution, the stabilization system would be able to operate to the limits of the integrated heater. Integrated heaters have been demonstrated to be able to tune to a magnitude sufficient enough to contend with changes in the ambient temperature of microelectronic environments [10, 12, 18], and hence, our stabilization system should be able to contend with the fluctuations in temperature expected for any commercial applications.

Acknowledgments